BaZr(0.8)Y(0.2)O(3-delta)-NiO Composite Anodic Powders for Proton-Conducting SOFCs Prepared by a Combustion Method

Lei Bi
National Institute for Materials Science, Japan

Emiliana Fabbri
National Institute for Materials Science, Japan

Ziqi Sun
University of Wollongong, ziqi@uow.edu.au

Enrico Traversa
National Institute for Materials Science, Japan

BaZr(0.8)Y(0.2)O(3-delta)-NiO Composite Anodic Powders for Proton-Conducting SOFCs Prepared by a Combustion Method

Abstract

$BaZr_{0.8}Y_{0.2}O_{3-\partial}$ (BZY)-NiO composite powders with different BZY-NiO weight ratios were prepared by a combustion method as anodes for proton-conducting solid oxide fuel cells (SOFCs). After heating to 1100°C for 6 h, the composite powders were made of a well-dispersed mixture of two phases, BZY and NiO. Chemical stability tests showed that the BZY-NiO anodic powders had good stability against CO_2, whereas comparative tests under the same conditions showed degradation for $BaCe_{0.7}Zr_{0.1}Y_{0.2}O_{3-\partial}$- NiO, which is at present the most used anode material for proton-conducting SOFCs. Area specific resistance (ASR) measurements for BZY-NiO anodes showed that their electrochemical performance depended on the BZY-NiO weight ratio. The best performance was obtained for the anode containing 50 wt % BZY and 50 wt % NiO, which showed the smallest ASR values in the whole testing temperature range (0.37 Ω cm2 at 600°C). The 50 wt % BZY and 50 wt % NiO anode prepared by combustion also showed superior performance than that of the BZY-NiO anode conventionally made by a mechanical mixing route, as well as that of Pt.

Keywords

bazr, combustion, 8, method, y, 2, o, 3, delta, nio, composite, anodic, powders, proton, conducting, sofcs, prepared

Disciplines

Engineering | Physical Sciences and Mathematics

Publication Details

BaZr$_{0.8}$Y$_{0.2}$O$_{3−\delta}$-NiO Composite Anodic Powders for Proton-Conducting SOFCs Prepared by a Combustion Method

Lei Bi, Emiliana Fabbri,[*] Ziqi Sun, and Enrico Traversa[*,z]

International Center for Materials Nanoarchitectnics, National Institute for Materials Science, Tsukuba, Ibaraki 305-0044, Japan

BaZr$_{0.8}$Y$_{0.2}$O$_{3−\delta}$ (BZY)-NiO composite powders with different BZY-NiO weight ratios were prepared by a combustion method as anodes for proton-conducting solid oxide fuel cells (SOFCs). After heating to 1100°C for 6 h, the composite powders were made of a well-dispersed mixture of two phases, BZY and NiO. Chemical stability tests showed that the BZY-NiO anodic powders had good stability against CO$_2$, whereas comparative tests under the same conditions showed degradation for BaCe$_{0.7}$Zr$_{0.1}$Y$_{0.2}$O$_{3−\delta}$-NiO, which is at present the most used anode material for proton-conducting SOFCs. Area specific resistance (ASR) measurements for BZY-NiO anodes showed that their electrochemical performance depended on the BZY-NiO weight ratio. The best performance was obtained for the anode containing 50 wt % BZY and 50 wt % NiO, which showed the smallest ASR values in the whole testing temperature range (0.37 Ω cm^2 at 600°C). The 50 wt % BZY and 50 wt % NiO anode prepared by combustion also showed superior performance than that of the BZY-NiO anode conventionally made by a mechanical mixing route, as well as that of Pt.
© 2011 The Electrochemical Society.   [DOI: 10.1149/1.3591040] All rights reserved.

Proton-conducting solid oxide fuel cells (SOFCs) have attracted much attention because they provide an effective way to lower the operating temperature of SOFCs.[1–4] Working at low temperatures requires not only the development of electrolyte materials with high ionic conductivity but also the development of cathode as well as anode materials that show good electrochemical performance at intermediate temperatures.[4–8] In the SOFC community, the most used anodes are the electrolyte-NiO composite materials,[9] also for proton-conducting SOFCs.[10,11] Comparing with the studies on electrolyte[12–14] and cathode materials,[15–17] studies on the anode material for proton-conducting SOFCs are only a few and focused on composite anodes made of NiO and barium (or strontium) cerate.[18–21] However, the poor chemical stability of alkaline earth cerates in CO$_2$ and H$_2$O containing atmosphere makes them unsuitable for practical applications.[3,22–26] On the other hand, doped BaZrO$_3$ shows good chemical stability against CO$_2$ and H$_2$O (Refs. [3] and [24]) and it gradually becomes a hot material as electrolyte for proton-conducting SOFCs.[27–29] Therefore, it is reasonable to assume that the BaZrO$_3$-NiO composite anode could show good chemical stability and has a great potential in fuel cell applications. In our recent study,[30] sinteractive BaZrO$_3$-NiO composite anode powders were successfully used to promote the densification of deposited BaZrO$_3$ films, demonstrating promise in fuel cell performance. Therefore, further thorough studies on the electrochemical properties of BaZrO$_3$-NiO anodes are desirable.

In addition, in the mentioned studies on anodes for proton-conducting SOFCs, there is a large scattering in the electrochemical performance of the anodes: the measured area specific resistance (ASR) values measured at the same temperature of 600°C varied between 0.06 Ω cm^2 and 10 Ω cm^2, although the anode compositions were almost similar.[18–20] This evidence suggests that the electrochemical performance of anodes based on protonic conductors deserve further attention.

Recent studies show that the microstructure of the anode is critical to SOFC performance.[31] The conventional mechanical mixing route for producing anode powders, which simply mix NiO and electrolyte materials together by ball milling, may result in an inhomogeneous distribution of the two phases. Moreover, wet chemical routes are regarded as effective ways to produce ultra-fine and uniform powders, which can enlarge the length of the triple-phase boundary (TPB) where electrochemical reactions occur.[32] Therefore, a combustion method was used in this study to prepare BaZr$_{0.8}$Y$_{0.2}$O$_{3−\delta}$ (BZY)-NiO composite anodic powders in one step with different BZY-NiO weight ratios. Microstructure and chemical

stability were studied for the BZY-NiO anode powders, and symmetrical cells were fabricated to investigate their electrochemical properties. An optimal composition between BZY and NiO was identified examining the performance of BZY-based anodes. The electrochemical performance of the BZY-NiO anode powders prepared by the combustion method was also compared with that of both Pt and BZY-NiO anode conventionally prepared by mixing, indicating that the combustion method provided a simple route to obtain stable and high performance BZY-NiO anodes for proton-conducting SOFCs.

Experimental

BaZr$_{0.8}$Y$_{0.2}$O$_{3−\delta}$ (BZY)-NiO composite anodic powders with different weight ratios (BZY:NiO = 20:80, 30:70, 40:60, 50:50 and 60:40) were synthesized in one step by a combustion method. Stoichiometric amounts of Ba(NO$_3$)$_2$ (99.9% purity, Wako), ZrO(NO$_3$)$_2$·2H$_2$O (97% purity, Wako), Y(NO$_3$)$_3$·6H$_2$O (99.8%, Aldrich) and (CH$_3$COO)$_2$·Ni·4H$_2$O (98% purity, Wako) were dissolved in distilled water. As a complexing agent, citric acid was then added, setting at 1.5 the molar ratio of citric acid/metal. NH$_4$OH was added to the solution to adjust the pH value around 8. The solution was heated under stirring and finally ignited to flame, resulting in a black ash. The ash was heated to 1100°C for 6 h to form fine BZY-NiO powders. From now on, BaZr$_{0.8}$Y$_{0.2}$O$_{3−\delta}$ (BZY)-NiO is named as BZY-NiO and acronym is followed by a number indicating the weight percentage of NiO in the composite powder, and BZY-Ni is used to describe its corresponding reduced state, also followed by a number indicating the NiO weight content in the original BZY-NiO powder. BaCe$_{0.7}$Zr$_{0.1}$Y$_{0.2}$O$_{3−\delta}$ (BCZY) electrolyte powder was also synthesized by the combustion method mentioned above, using Ba(NO$_3$)$_2$, Ce(NO$_3$)$_3$·6H$_2$O, ZrO(NO$_3$)$_2$·2H$_2$O, and Y(NO$_3$)$_3$·6H$_2$O as the starting materials. The BCZY powder was heated to 1000°C for 6 h. X-ray diffraction (XRD, Rigaku, with Cu Ka radiation) analysis was used to identify the phase structures of the as-prepared powders. Thermogravimetric (TG, NETZSCH STA 409C/CD) analysis in CO$_2$ atmosphere was carried out to investigate the chemical stability of BZY-NiO anodic powders at a heating rate of 10°C min^{-1}. The TG measurements were held at 700°C for 3 h and 100% CO$_2$ was used as the flowing gas at a rate of 100 ml min^{-1}. For comparison, BCZY-NiO composite anodic powder was tested in the same environment. The phase composition of these powders after TG test was analyzed by XRD.

Symmetrical anode/electrolyte/anode assemblies were fabricated by a co-pressing technique. The BCZY powder was first pressed at 100 MPa. Then the BZY-NiO anode powder was directly deposited on the green BCZY surface and pressed at 150 MPa before fabricating the second BZY-NiO layer at the opposite face of the BCZY electrolyte that was pressed at 200 MPa. The diameter of the green pellets was 13 mm. The tri-layer assemblies were fired at 1400°C

for 6 h to form the symmetrical cells with anode layer at both sides of the electrolyte. The symmetrical cells were firstly heated to 700°C and kept at 700°C in a wet 20% H_2 in Ar atmosphere (~3% H_2O) for 2 h to reduce the anode before electrochemical testing. The cells were then tested in a wet 20% H_2 in Ar atmosphere (~3% H_2O) at a flowing rate of 50 ml min^{-1} using a multichannel potentiostat (VMP3 Bio-Logic Co.) in the frequency range between from 0.1 Hz to 1 MHz, with an AC voltage amplitude of 100 mV. The impedance spectra were fitted with Zview software.

Scanning electron microscopy (SEM, Hitachi S-4800) was used to observe the morphologies of anode layers after reduction. Energy dispersive X-ray spectroscopy (EDS) analysis was used to examine the possible element diffusion at the anode/electrolyte interface. Symmetrical cells with Pt (Nilaco Co., Japan) and BZY-NiO (commercial NiO was purchased from Wako) electrodes prepared by the conventional mechanical mixing route in which BZY powder was mixed with commercial NiO in a weight ratio of 1:1 by ball-milling in ethanol for 24 h and then dried at 90°C overnight to evaporate the ethanol were also fabricated and tested in the same conditions to compare their performance with the BZY-NiO anodic powders made by the combustion method.

Results and Discussion

Powder characterization.— Figure 1 shows the XRD patterns of the composite anodic powders with different BZY-NiO weight ratios prepared by a combustion method, showing only the presence of BZY and NiO phases. The difference in the weight ratio between BZY and NiO just changed the relative intensity of the two phases in the XRD patterns. It has been reported that a small amount of Ni can be substituted in the BZY lattice and the doping can occur during the mechanical mixing and high temperature firing process.[33,34] A small amount of Ni may introduce some electronic conductivity in the BZY samples[33] and this electronic conductivity can be even beneficial to promote the anode reaction. In addition, the Ni-modified BZY was reported to show improved protonic conductivity according to research of Tong et al.[34] Nonetheless, no obvious secondary phases could be observed in the XRD patterns of BZY-NiO anodes after firing, and the lattice parameter for BZY in the composite anodic powders almost kept constant at around 4.215 Å, in agreement with the BZY lattice parameter reported in the literature [from 4.21 Å (Ref. 35) to 4.23 Å (Ref. 36)], indicating that the NiO content in the composite powders did not alter the lattice structure of BZY in the

composite anodic powders. Figure 2 shows the XRD patterns for the BZY-NiO anode pellets sintered at 1400°C for 6 h, indicating the phase of these anodes remained unchanged during the high temperature firing, in spite of the formation of a small amount of BaY_2NiO_5.[30,34]

Figure 3 shows the back scattering electron (BSE) SEM micrograph of the BZY-NiO powder in the 20:80 weight ratio after heating to 1100°C for 6 h, indicating clearly the presence of two different phases in the composite anode powders. The particle size of NiO (dark particles) was about 500 nm and the particle size of BZY (light particles) was about 50 nm. The same morphology was observed for the other composite samples, with the only change of the phase relative amounts.

Chemical stability.— The problem of chemical stability is a main challenge for proton conducting oxides. A previous report[20] demonstrated that the $BaCeO_3$-NiO composite anode showed inadequate chemical stability against CO_2. Doping with Zr has been used to improve the chemical stability of $BaCeO_3$-based materials; after the work of Zuo et al.[13] who reported that 10% Zr doping in $BaCeO_3$ ($BaCe_{0.7}Zr_{0.1}Y_{0.2}O_{3-\delta}$, BCZY) improved its chemical stability, BCZY became the most used electrolyte material for proton-conducting SOFCs as well as its counterpart anode.[13,15] However, several reports[26,37,38] showed that BCZY has insufficient chemical stability in real fuel-cell conditions. In the present study, the chemical stability of two BZY-NiO compositions (BZY-NiO50 and BZY-NiO60 anodic powders) was tested, together with that of BCZY-NiO anodic powder in a 50:50 weight ratio, for sake of comparison. Figure 4 shows the TG curves for BCZY-NiO, BZY-NiO50 and BZY-NiO60 powders as a function of time and temperature, measured in pure CO_2. The samples were heated from room temperature to 700°C and held at 700°C for 3 h under pure CO_2 flowing. An increase in weight for the BCZY-NiO powder was clearly observed, ascribed to the reaction between BCZY and CO_2 during the test,[23,37] leading to the formation of barium carbonate. On the contrary, the weight of BZY-NiO50 and BZY-NiO60 did not increase, implying that there was no reaction between BZY-NiO anode materials and CO_2. The slight weight decrease observed for both these anode compositions can be ascribed to sample dehydration.

XRD analysis further confirmed the conclusion that the BZY-NiO powders did not react with CO_2 after the TG test in CO_2 atmosphere. Figure 5 shows the XRD patterns of BCZY-NiO, BZY-NiO50 and BZY-NiO60 powders before and after CO_2
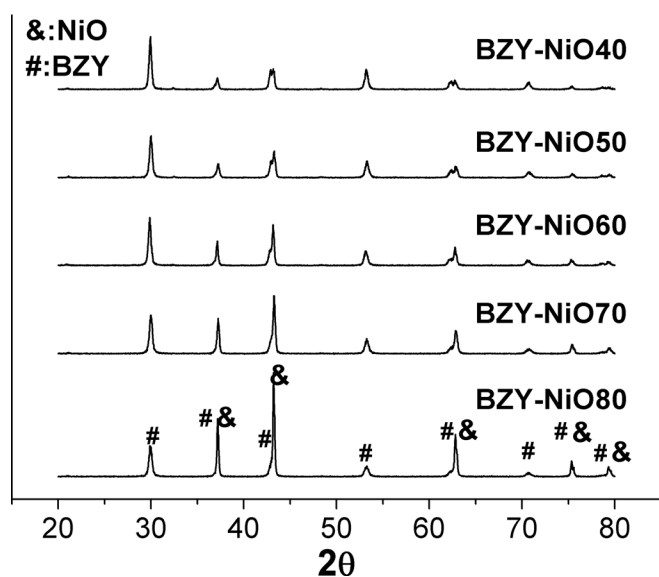

Figure 1. XRD patterns for composite powders with different BZY-NiO weight ratio fired at 1100 °C for 6 h.
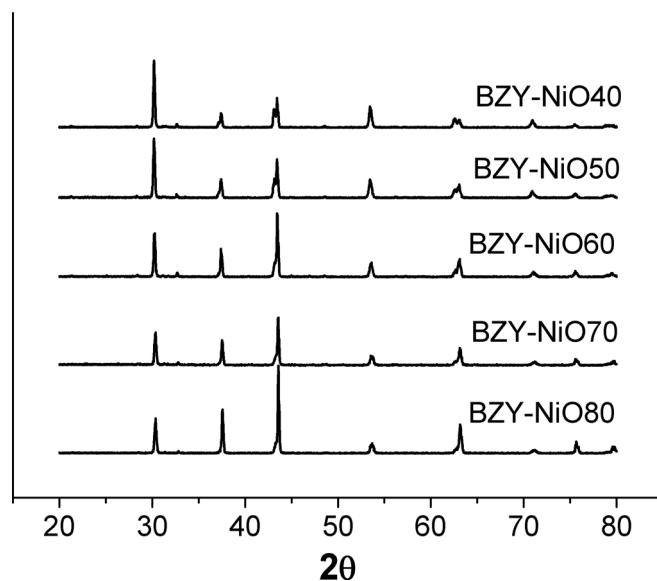

Figure 2. XRD patterns for composite BZY-NiO anode pellets sintered at 1400 °C for 6 h.
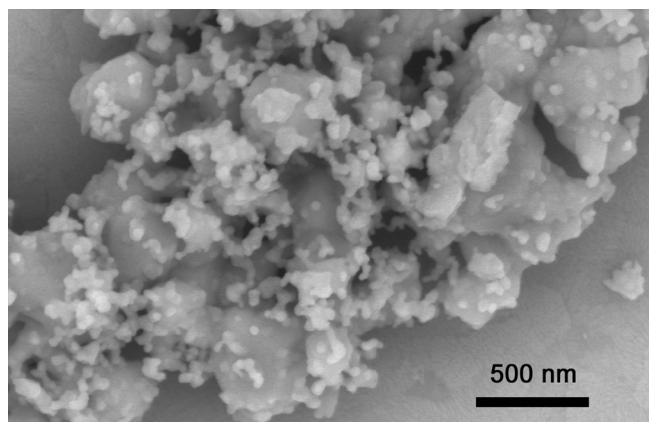
Figure 3. Back scattering electron (BSE) image of typical BZY-NiO powder in the weight ratio of 20:80 prepared by a combustion method after firing at 1100 °C for 6 h.

exposure. The as-prepared BCZY-NiO sample consisted in BCZY and NiO phases. After exposure to CO_2, the XRD pattern shows that the NiO reflection lines remained unchanged, suggesting no chemical degradation of the NiO phase, whereas large peaks of $BaCO_3$ and CeO_2 appeared with no BCZY peaks, indicating the complete BCZY decomposition, in agreement with the TG measurements. Instead, the XRD patterns of both BZY-NiO50 and BZY-NiO60 kept unchanged after CO_2 exposure, showing good chemical stability for the BZY-NiO anode materials. These findings suggest that the chemical stability of BCZY-NiO against CO_2 is insufficient for fuel cell applications in operating conditions, despite its wide use in the laboratory for proton-conducting SOFCs, while the BZY-NiO composite anode shows excellent chemical stability and has a better potential for fuel cell applications.

Electrochemical analysis.— The electrochemical properties of the BZY-NiO anodes were characterized in symmetrical cells using an electrolyte pellet with an anode layer deposited on both sides. Despite its insufficient chemical stability, BCZY was selected as electrolyte for symmetrical cell testing for two reasons: to make a comparison with other anodes reported in the relevant literature that were studied with this same electrolyte, and to exploit the good BCZY sintering activity that allows fabricating dense BCZY electrolyte pellets (1 mm in thickness) during the co-firing with the anode layers at 1400°C, whereas $BaZrO_3$ pellets were still porous. Figure 6 shows the SEM fracture micrographs of anode/electrolyte bi-layers after NiO reduction. BZY-Ni films with a thickness of
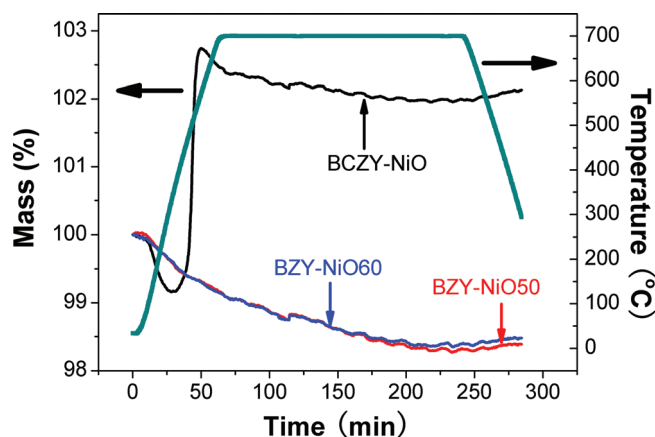

Figure 4. (Color online) TG curves for $BaCe_{0.7}Zr_{0.1}Y_{0.2}O_{3-\delta}$ (BCZY)-NiO, BZY-NiO50 and BZY-NiO60 composite powders, measured in pure CO_2 atmosphere.
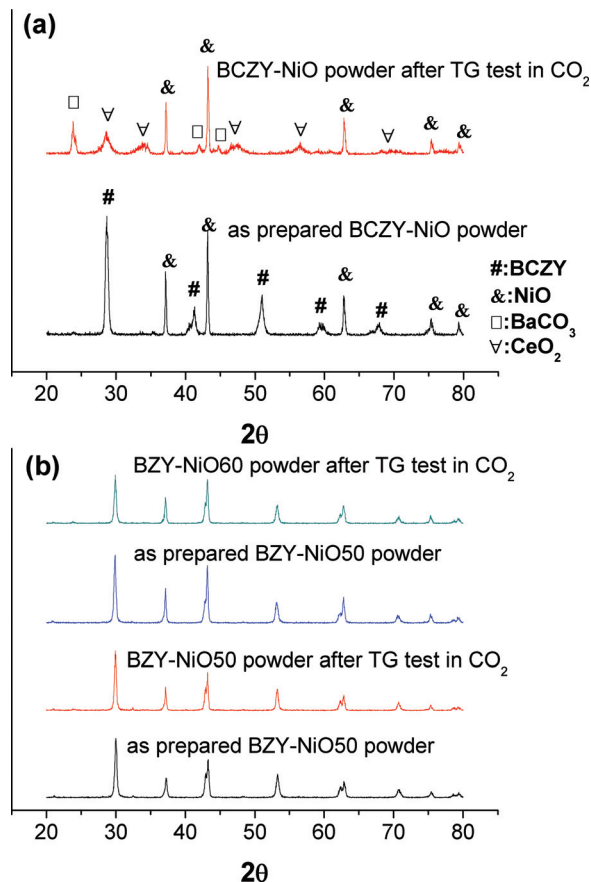

Figure 5. (Color online) XRD patterns for (a) BCZY-NiO powder, and (b) BZY-NiO50, BZY-NiO60 powders before and after the TG test in pure CO_2.

about 70 μm were obtained on dense BCZY electrolytes. The anode layers attached well with the electrolyte and there was no cracking or delamination after reduction. Figure 7 shows the high-magnification SEM micrographs of the composite BZY-Ni anode layer,
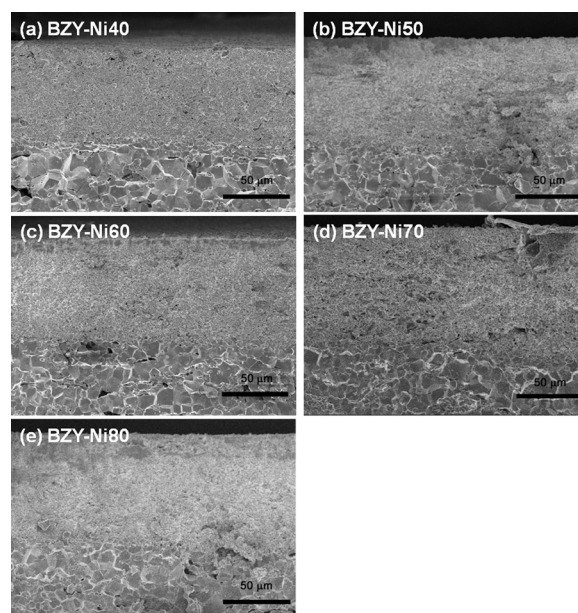

Figure 6. SEM cross-sectional micrographs of the electrolyte/anode interface for composite powders with different BZY-NiO weight ratio, after reduction in hydrogen.
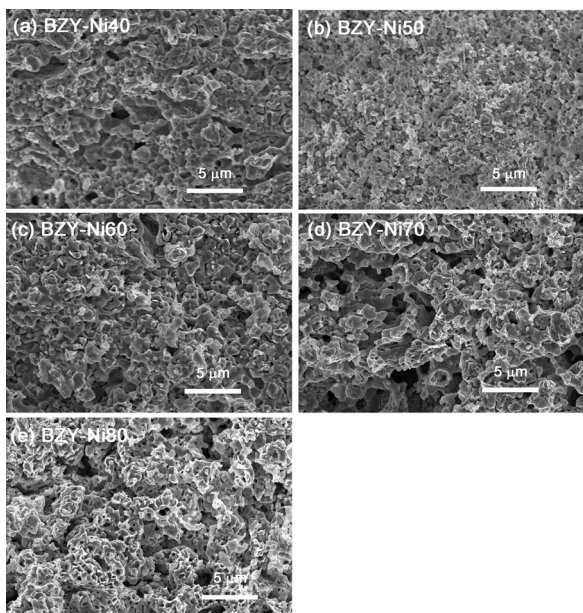
Figure 7. High-magnification SEM cross-sectional micrographs of the composite anode layer with different BZY-NiO weight ratio, after reduction in hydrogen.

indicating that the anode layers were well reduced and presented a porous structure. Figure 8 shows the SEM-EDS elemental analysis of Ce and Zr in line-scan mode of the BZY-NiO anode film/BCZY electrolyte interface after firing at 1400°C, performed to check the possible Zr-Ce diffusion due to the Zr and Ce concentration gradient between the two materials. The Ce signal is small in the anode and increases in the BCZY electrolyte. The change in Ce concentration in the BCZY electrolyte is not abrupt, but Ce concentration gradually increased from the interface into the electrolyte side, reaching a constant value of Ce concentration at a thickness of about 10 μm. A gradual Zr concentration decrease corresponded to the gradual Ce concentration increase, showing the presence of a diffusion layer about several micrometers in thickness. The inter-diffusion between Zr and Ce was expected since many reports[23–26] indicated that $BaCeO_3$ and $BaZrO_3$ can form solid solutions. Partial diffusion of Zr from BZY-based anode to BCZY electrolyte can enhance its chemical stability owing to the formation of an outer electrolyte layer with larger Zr content than that of the original BCZY material exposed to the anode side, having better chemical stability[25,26] and
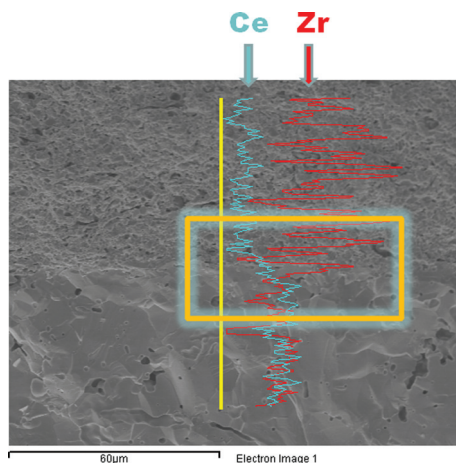

Figure 8. (Color online) SEM-EDS elemental analysis of Ce and Zr in line-scan mode at the interface of the electrolyte and anode.
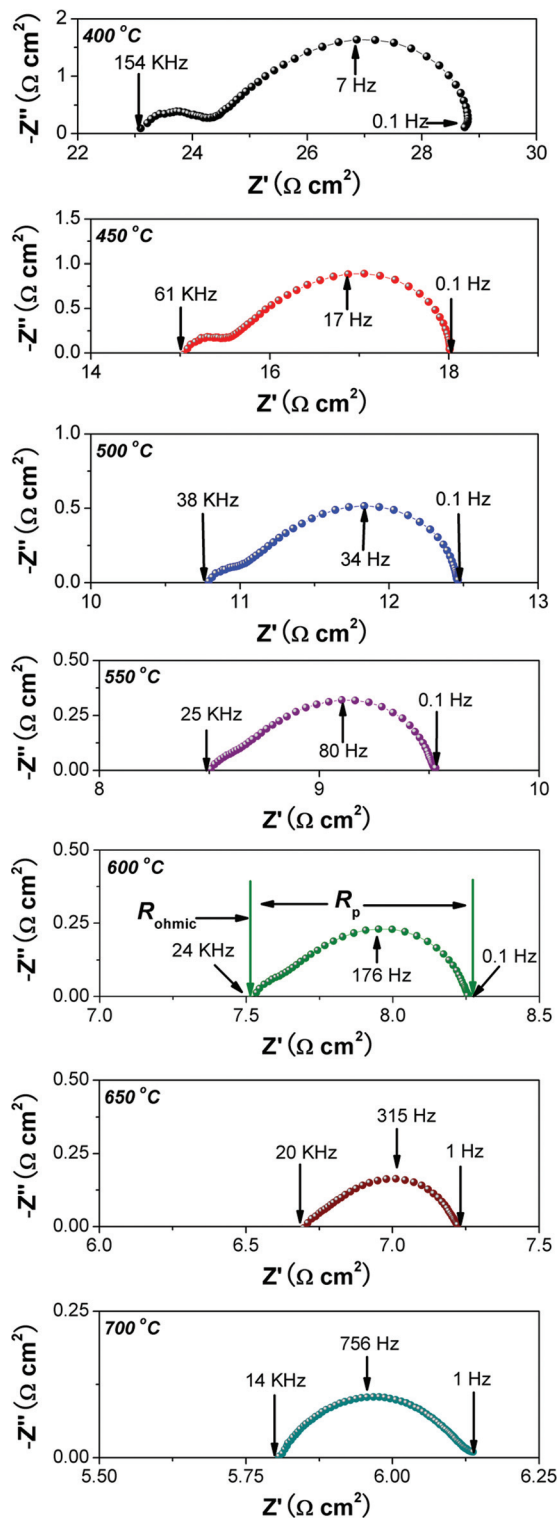

Figure 9. (Color online) Complex-impedance plane plots for the symmetrical cell with BZY-Ni50 anodes measured at different temperatures in a wet 20% H_2-containing atmosphere.

may serve as a protective layer for the bulk electrolyte. Similar diffusion results were also observed by Meulenberg et al.[39]

Figure 9 shows the typical electrochemical impedance spectroscopy (EIS) plots of the symmetrical cell with BZY-NiO50 anode, measured from 400 to 700°C in wet 20% H_2 (∼3% H_2O). At very low temperatures (such as 200°C), there were another two additional semicircles at high frequencies, which were attributed to bulk and
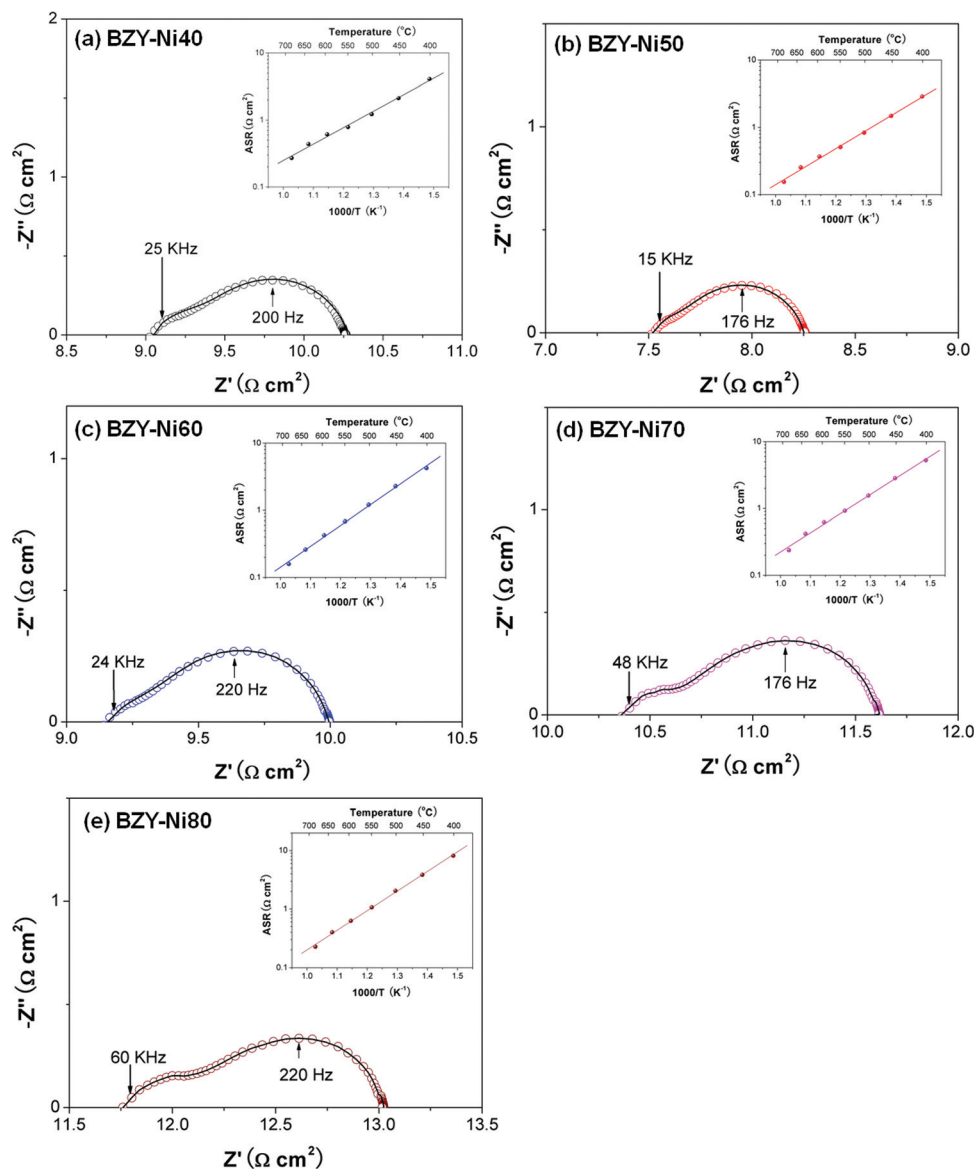
Figure 10. (Color online) Complex-impedance plane plots of BZY-Ni anodes with different NiO content in the anodic powders measured at 600 °C in a wet 20% H_2-containing atmosphere (the circles present the experimental data and the solid lines are the fitted curves). The insets display the Arrhenius plots of the ASR values for the corresponding anodes.

grain boundary contributions. With the increase of the temperatures, the two arcs merged into one semicircle and finally led to a high frequency resistance. The intercept with the real axis at high frequency represents the ohmic resistance (R_{ohmic}) of the cell, which includes the electrolyte and lead wire resistances. The low frequency intercept corresponds to the total resistance of the cell. Therefore, the difference between the high frequency and low frequency intercepts with the real axis represents the polarization resistance (R_p) of the cell. It can be seen that the R_p values decreased with increasing the temperature. The area specific resistance (ASR) of the anodes was calculated from the electrode polarization resistance (R_p) as ASR $= (R_p A)/2$, where A is the geometrical electrode area and the factor $1/2$ takes into consideration that symmetrical cells were used.[20,40]

Figure 10 shows the EIS plots of the BZY-Ni anodes with different Ni content measured at 600°C in a wet 20% H_2 (~3% H_2O) atmosphere. The insets display the temperature dependence of ASR values for these BZY-Ni anodes. At 600°C, ASR values of 0.61, 0.37, 0.43, 0.62 and 0.63 Ω cm^2 were obtained for the BZY-Ni40, BZY-Ni50, BZY-Ni60, BZY-Ni70 and BZY-Ni80 composite anodes, respectively. The ASR values decreased dramatically for each

specimen with increasing the measuring temperature. As shown in Fig. 11, the BZY-Ni50 anode showed the best electrochemical performance in the whole testing temperature range, indicating that the best weight composition for BZY and NiO is 50:50. The performance of the BZY-NiO50 anode prepared by the combustion method was also better than that of Pt as well as that of the BZY-NiO anode conventionally prepared by a mechanical mixing route, as shown in Fig. 12. Figure 12a shows that the ASR values measured for Pt electrode in the whole temperature range was much larger than that of the BZY-Ni50 anode, indicating that Pt might not be a good choice as the anode for barium zirconate electrolytes, in agreement with the literature.[22,23] Figure 12b shows the ASR values of BZY-Ni50 anodes prepared by the combustion method and the mechanical mixing route. The anode prepared by the combustion method showed smaller ASR values than those measured for the anode prepared by the conventional mechanical mixing procedure, though having the same composition. The smaller difference at low temperatures may result from the better sintering activity for the combustion BZY-Ni50 anode that led to a smaller porosity compared with that of the conventional anode. The better performance for the anode prepared by the combustion method is due to a better microstructure made by
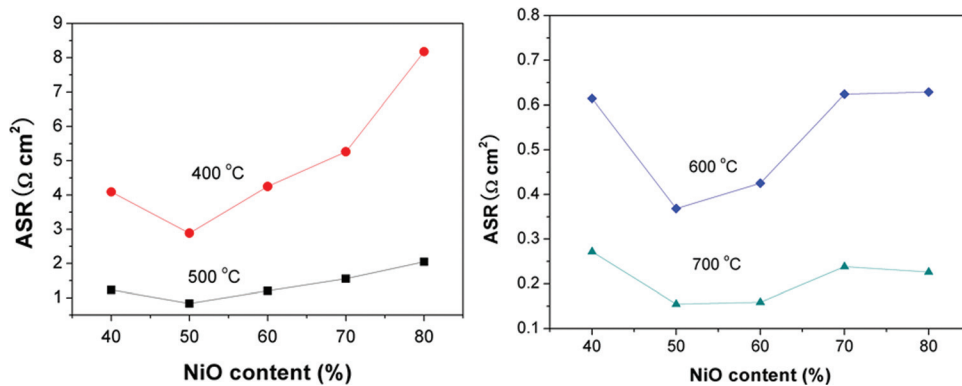
Figure 11. (Color online) ASR values of the composite anodes as a function of NiO weight content at different temperatures.

the one-step combustion method, with a more uniform distribution of BZY and Ni particles as well as smaller Ni particle size, which is illustrated in Fig. 13 that shows a SEM micrograph of the two anodes. A homogeneous distribution of small particles in the BZY-Ni anode prepared by the combustion method effectively enlarged the length of the triple-phase boundary (TPB) and thus led to a smaller electrode polarization resistance.

The BZY-Ni50 anode prepared by combustion showed a better electrochemical performance than that of most of the proton conductor-based anodes for proton-conducting SOFCs reported in the literature.[18,20] However, better performance was reported for an anode made of Ni and $BaCe_{0.9}Y_{0.1}O_{3-\delta}$ (BCY) nanopowders,[19] which might have problems of chemical stability in fuel cell applications. The activation energy of the BZY-Ni50 anode was 0.53 eV, slightly larger than that of cerate proton conductor based anodes [such as $BaCe_{0.9}Y_{0.1}O_{3-\delta}$-Ni with the activation energy of 0.32eV (Ref. 20) and $SrCe_{0.9}Yb_{0.1}O_{3-\delta}$-Ni with the activation energy of 0.4eV (Ref. 18)], in agreement with the slightly larger activation energy of doped-$BaZrO_3$ with respect to doped $BaCeO_3$.[23]

Figures 9 and 10 clearly show the presence of two depressed semi-circles in each EIS plot, indicating two different electrochemical mechanisms. A thorough analysis of the EIS data was performed to unravel the possible electrochemical reactions occurring at the anode and affecting the ASR. The equivalent circuit used to fit the impedance spectra was made of a resistance and an inductance associated in series with two distributed elements, composed by a constant phase element in parallel with a resistance. Similar circuits have been widely used previously for SOFC anode studies.[32] The ASR is the sum of the contributions of the resistance calculated from the semicircle at the high frequency (ASR_{HF}) and the resistance calculated from the semicircle at the low frequency (ASR_{LF}). With increasing the temperature, the diameter of both semi-circles gradually decreased and the high frequency semi-circle tended to disappear at high temperatures (above 600°C). Therefore, we separated the contribution of ASR_{HF} and ASR_{LF} obtained from the EIS plots for BZY-NiO anodes with different BZY-NiO weight ratios in the 400–600°C temperature range (Fig. 14). The ASR_{HF} activation energy for the BZY-Ni anodes was between 0.44 and 0.65 eV. These activation energy values were within the range of values reported in the literature for proton conduction in oxides,[3,14,23,25] suggesting that protons are involved in the electrochemical reactions. Moreover, the semi-circle at high frequency showed a capacitance value in the order of 10^{-5} F cm^{-2}, which is usually associated to charge transfer processes at the electrode/electrolyte interface.[41,42] Therefore, the ASR_{HF} was ascribed to proton migration at the anode/electrolyte interface. The semi-circles at low frequency, related to ASR_{LF}, showed capacitance values in the order of 10^{-3} F cm^{-2}. The larger capacitance compared with that at high frequency is usually associated with surface reactions.[40,42] Therefore, it is reasonable to assume that the ASR_{LF} for the anode is related to the
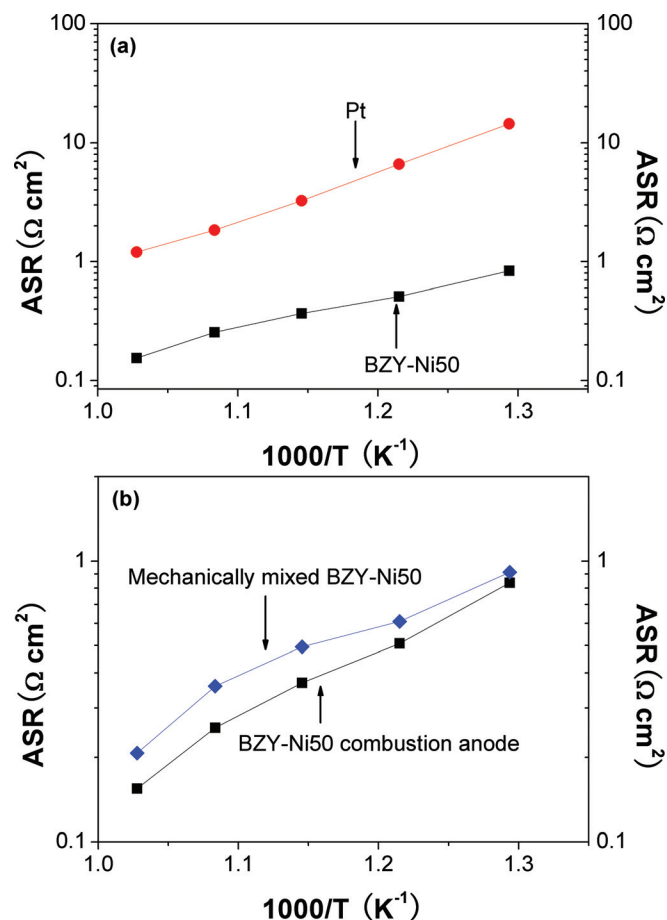

Figure 12. (Color online) Comparison of ASR values of (a) BZY-Ni50 combustion anode and Pt anode, and (b) BZY-Ni50 anodes prepared by the combustion method and by the mechanical mixing route.
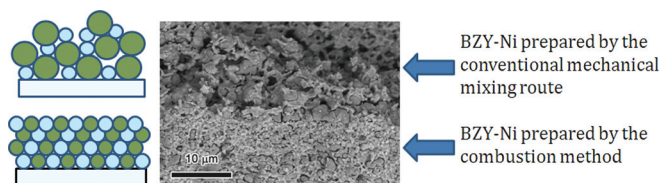

Figure 13. (Color online) SEM micrograph for BZY-Ni anodes prepared by the combustion method and conventional mechanical mixing route, with a schematic diagram of particle distribution.
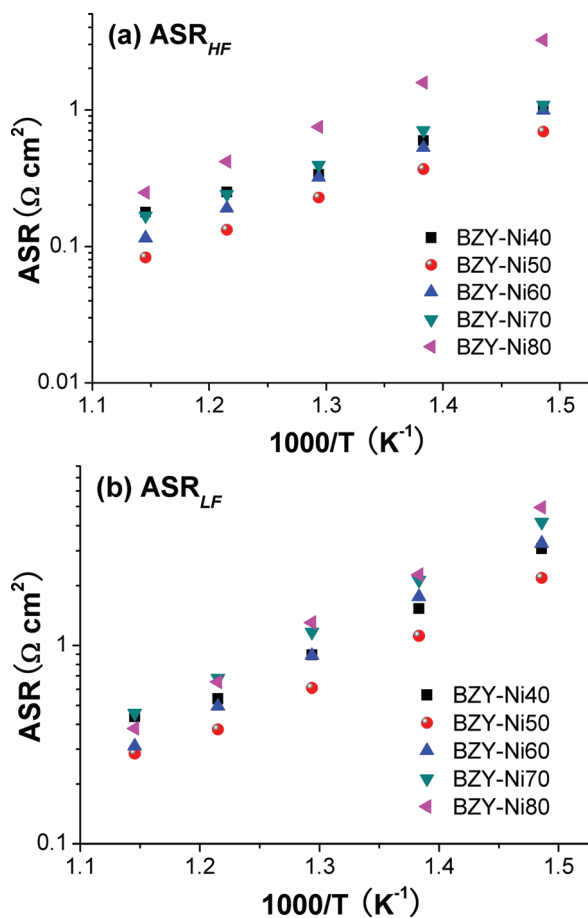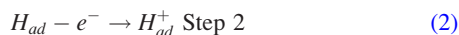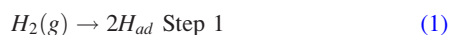
Figure 14. (Color online) (a) ASR_{HF} and (b) ASR_{LF} temperature dependence for composite anodes with different NiO weight contents in a wet 20% H_2-containing atmosphere.

dissociative adsorption of the fuel gas at the anode side, herein H_2. The reaction can be written as

$$H_2(g) \rightarrow 2H_{ad} \text{ Step 1} \tag{1}$$

$$H_{ad} - e^- \rightarrow H_{ad}^+ \text{ Step 2} \tag{2}$$

Although the anode containing 50 wt % BZY and 50 wt % NiO also shows the lowest ASR_{LF} values in the testing temperature range, the value of ASR_{LF} is obviously larger than that of the ASR_{HF} at the same temperature and the same trend was observed for the other compositions. The similar phenomenon of large ASR_{LF} was observed for the literature reported BCY-NiO anode.[20] The larger ASR_{LF} with respect to ASR_{HF} suggests that the dissociative adsorption of H_2 is the rate limiting step for the composite BZY-NiO anode.

Conclusions

A combustion method was used to prepare BZY-NiO anodic powders with different BZY-NiO weight ratios for proton conducting SOFCs. Compared with the most utilized BaCeO$_3$-based composite anodic powder, BZY-NiO showed comparable electrochemical performance but much improved chemical stability, and has potential for application in practical fuel cell operating conditions. ASR values obtained from symmetrical cell measurements indicated that the optimized composition between BZY and NiO for the combustion anode is 50:50, which showed the lowest polarization resistance among all the compositions. EIS analysis suggested that there were two different electrochemical mechanisms occurring at the anode, being dissociative adsorption of H_2 the rate limiting

step. In addition, the BZY-NiO50 anode in the present study also showed lower polarization resistance than most of the proton conductor-NiO composite anodes previously reported and possessed much better chemical stability. The desirable electrochemical performance and excellent chemical stability make the BZY-NiO anodes prepared by the combustion method promising for proton-conducting SOFCs.

References

1. H. Iwahara, H. Uchida, and K. Morimoto, *J. Electrochem. Soc.*, **137**, 462 (1990).
2. T. Norby, *Solid State Ionics*, **125**, 1 (1999).
3. K. D. Kreuer, *Annu. Rev. Mater. Res.*, **33**, 333 (2003).
4. E. Fabbri, D. Pergolesi, and E. Traversa, *Chem. Soc. Rev.*, **39**, 4355 (2010).
5. E. Fabbri, A. D'Epifanio, S. Sanna, E. Di Bartolomeo, G. Balestrino, S. Licoccia, and E. Traversa, *Energy Environ. Sci.*, **3**, 618 (2010).
6. L. Bi, Z. T. Tao, R. R. Peng, and W. Liu, *J. Inorg. Mater.*, **25**, 1 (2010).
7. L. Bi, S. Q. Zhang, S. M. Fang, L. Zhang, H. Y. Gao, G. Y. Meng, and W. Liu, *J. Am. Ceram. Soc.*, **91**, 3806 (2008).
8. E. Fabbri, D. Pergolesi, and E. Traversa, *Sci. Technol. Adv. Mater.*, **11**, 044301 (2010).
9. A. Orera and P. R. Slater, *Chem. Mater.*, **22**, 675 (2010).
10. D. Pergolesi, E. Fabbri, and E. Traversa, *Electrochem. Commun.*, **12**, 977 (2010).
11. L. Bi, Z. T. Tao, W. P. Sun, S. Q. Zhang, R. R. Peng, and W. Liu, *J. Power Sources*, **191**, 428 (2009).
12. S. W. Tao and J. T. S. Irvine, *Adv. Mater.*, **18**, 1581 (2006).
13. C. D. Zuo, S. W. Zha, M. L. Liu, M. Hatano, and M. Uchiyama, *Adv. Mater.*, **18**, 3318 (2006).
14. R. Haugsrud and T. Norby, *Nature Mater.*, **5**, 193 (2006).
15. L. Yang, C. D. Zuo, S. Z. Wang, Z. Cheng, and M. L. Liu, *Adv. Mater.*, **20**, 3280 (2008).
16. E. Fabbri, T. K. Oh, S. Licoccia, E. Traversa, and E. D. Wachsman, *J. Electrochem. Soc.*, **156**, B38 (2009).
17. G. Taillades, J. Dailly, M. Taillades-Jacquin, F. Mauvy, A. Essouhmi, M. Marrony, C. Lalanne, S. Fourcade, D. J. Jones, J. C. Grenier et al., *Fuel Cells*, **10**, 166 (2010).
18. G. C. Mather, F. M. Figueiredo, D. P. Fagg, T. Norby, J. R. Jurado, and J. R. Frade, *Solid State Ionics*, **158**, 333 (2003).
19. A. Essoumhi, G. Taillades, M. Taillades-Jacquin, D. J. Jones, and J. Roziere, *Solid State Ionics*, **179**, 2155 (2008).
20. L. Chevallier, M. Zunic, V. Esposito, E. Di Bartolomeo, and E. Traversa, *Solid State Ionics*, **180**, 715 (2009).
21. M. Zunic, L. Chevallier, A. Radojkovic, G. Brankovic, Z. Brankovic, and E. Di Bartolomeo, *J. Alloys Compd.*, **509**, 1157 (2011).
22. E. Fabbri, D. Pergolesi, A. D'Epifanio, E. Di Bartolomeo, G. Balestrino, S. Licoccia, and E. Traversa, *Energy Environ. Sci.*, **1**, 355 (2008).
23. E. Fabbri, A. D'Epifanio, E. Di Bartolomeo, S. Licoccia, and E. Traversa, *Solid State Ionics*, **179**, 558 (2008).
24. Z. M. Zhong, *Solid State Ionics*, **178**, 213 (2007).
25. K. Katahira, Y. Kohchi, T. Shimura, and H. Iwahara, *Solid State Ionics*, **138**, 91 (2000).
26. Y. M. Guo, Y. Lin, R. Ran, and Z. P. Shao, *J. Power Sources*, **193**, 400 (2009).
27. J. M. Serra and W. A. Meulenberg, *J. Am. Ceram. Soc.*, **90**, 2082 (2007).
28. D. Pergolesi, E. Fabbri, A. D'Epifanio, E. Di Bartolomeo, A. Tebano, S. Sanna, S. Licoccia, G. Balestrino, and E. Traversa, *Nature Mater.*, **9**, 846 (2010).
29. L. Bi, E. Fabbri, Z. Q. Sun, and E. Traversa, *Energy Environ. Sci.*, **4**, 409 (2011).
30. L. Bi, E. Fabbri, Z. Q. Sun, and E. Traversa, *Energy Environ. Sci.*, **4**, 1352 (2011).
31. T. Suzuki, Z. Hasan, Y. Funahashi, T. Yamaguchi, Y. Fujishiro, and M. Awano, *Science*, **325**, 852 (2009).
32. M. Chen, B. H. Kim, Q. Xu, and B. G. Ahn, *J. Membr. Sci.*, **334**, 138 (2009).
33. P. Babilo and S. M. Haile, *J. Am. Ceram. Soc.*, **88**, 2362 (2005).
34. J. H. Tong, D. Clark, M. Hoban, and R. O'Hayre, *Solid State Ionics*, **181**, 496 (2010).
35. E. Fabbri, D. Pergolesi, S. Licoccia, and E. Traversa, *Solid State Ionics*, **181**, 1043 (2010).
36. Y. Yamazaki, R. Hernandez-Sanchez, and S. M. Haile, *J. Mater. Chem.*, **20**, 8158 (2010).
37. L. Bi, Z. T. Tao, C. Liu, W. P. Sun, H. Q. Wang, and W. Liu, *J. Membr. Sci.*, **336**, 1 (2009).
38. E. Fabbri, L. Bi, H. Tanaka, D. Pergolesi, and E. Traversa, *Adv. Funct. Mater.*, **21**, 158 (2011).
39. W. A. Meulenberg, J. M. Serra, and T. Schober, *Solid State Ionics*, **177**, 2851 (2006).
40. E. Fabbri, S. Licoccia, E. Traversa, and E. D. Wachsman, *Fuel Cells*, **9**, 128 (2009).
41. V. Dusastre and J. A. Kilner, *Solid State Ionics*, **126**, 163 (1999).
42. F. He, T. Z. Wu, R. R. Peng, and C. R. Xia, *J. Power Sources*, **194**, 263 (2009).